J Nanopart Res (2015) 17:432
DOI 10.1007/s11051-015-3231-y

RESEARCH PAPER

Diamagnetic, paramagnetic, and ferromagnetic properties of ball milled $Bi_{1.65}Pb_{0.35}Sr_2Ca_2Cu_3O_{10+\delta}$ powders

E. Govea-Alcaide · L. Pérez-Acosta · P. K. Kiyohara · R. F. Jardim

Received: 29 May 2015 / Accepted: 22 October 2015 / Published online: 3 November 2015

Abstract We have performed a systematic study of the general physical properties of $(Bi,Pb)_2Sr_2Ca_2Cu_{10+y}$ (Bi-2223) powders that were ball milled for time intervals of up to $t_m = 210$ min. X-ray powder diffraction diagrams indicate that the phase composition of the samples seems to be preserved after the ball milling process, but the average grain size of the samples decreases appreciably with increasing milling time t_m. For $t_m = 120$ min, the transmission electron microscopy (TEM) images revealed the presence of Bi-2223 grains in the form of nanorods with a mean diameter of $d_g \sim 20$ nm. The temperature dependence of the magnetic susceptibility, $\chi(T)$, showed the occurrence of superconductivity below $T_c \sim 108$ K in all samples studied and a progressive decrease of the diamagnetic contribution to $\chi(T)$ with increasing t_m. Such a decrease in the diamagnetic contribution to $\chi(T)$ is accompanied by an increase of a paramagnetic contribution that has its origin in a disordered shell of the milled grains. Increasing t_m results in a progressive increase of the width of disordered shell further increasing the paramagnetic contribution to $\chi(T)$ that shows a very small diamagnetic component in samples subjected to large milling times. We have also found that the occurrence of oxygen vacancies in the disordered shell is responsible for a ferromagnetic contribution to $\chi(T)$ at high temperatures. Such a shell–core morphology of the milled grains, comprising a superconducting and diamagnetic core and a disordered and paramagnetic shell, is sufficient for interpreting the magnetic properties of the samples.

Keywords Ball milling · Bi-2223 superconductor · Diamagnetic contribution · Magnetic susceptibility · Nanopowders

E. Govea-Alcaide (✉)
Departamento de Física-Matemática, Facultad de Ciencias Informáticas, Naturales y Exactas, Universidad de Granma, Apdo. 21, P. O. Box 85100, Bayamo, Cuba
e-mail: egoveaa@udg.co.cu

L. Pérez-Acosta
Departamento de Física, Facultad de Electromecánica, Universidad de Camagüey, Circunvalación Norte Km 5 1/2 s/n, Camagüey, Cuba

P. K. Kiyohara · R. F. Jardim
Instituto de Física, Universidade de São Paulo, CP 66318, São Paulo, SP 05315-970, Brazil

Introduction

Studies of nanoparticles (NPs) have become a very active area of research because of their unique properties. In particular, the experiments performed by Ralph et al. (1995), Black et al. (1996) in nanometer-size Al superconducting grains have stimulated a great number of experimental and theoretical works (Di Lorenzo et al. 2000; Reich et al. 2003). This is supported by the fact that the superconducting

properties are altered when any size of a superconducting material is reduced to near or less than the London penetration depth, $\lambda_L(T)$, or the coherence length, $\xi(T)$. For example, variations of the critical temperature, T_c (Bose et al. 2005), and the superconducting pairing correlations (Di Lorenzo et al. 2000; Von Delft 2001) have been observed in nanosized superconducting specimens. However, most of the experimental studies on superconducting powder specimens were conducted in samples of elemental superconductors such as Al (Ralph et al. 1995; Black et al. 1996), Pb (Reich et al. 2003), and Nb (Bose et al. 2005) mainly due to their simple crystal structures, and the readiness in obtaining nanoparticles free of impurities and extra phases. On the other hand, it is also well known that only few studies on small-particle size samples have been conducted in the normal and superconducting properties of high-temperature high-T_c superconducting cuprates. On this subject, the synthesis and the general physical properties of $La_{1.85}Sr_{0.15}CuO_4$ nanorods prepared by the sol–gel template method have been reported Lu et al. (2007). Also, a systematic study of $YBa_2Cu_3O_{6+x}$ (YBCO) nanopowders, prepared by the citrate sol–gel method, has been conducted by Paturi et al. (2003). The authors found that the magnetic susceptibility $\chi(T)$ of the samples strongly varied with the size of the small particles, as expected from theoretical calculations (Paturi et al. 2003). More recently, studies conducted in a large variety of inorganic nanoparticles have revealed the very common occurrence of room-temperature ferromagnetism although the materials are intrinsically nonmagnetic, including here the superconducting cuprates (Sundaresan and Rao 2009). We also mention that systems comprising YBCO nanoparticles exhibit a ferromagnetic contribution at room temperature (Sundaresan and Rao 2009; Shipra et al. 2007; Hasanain et al. 2010; Arabi et al. 2013; Gasmi et al. 2013). Moreover, these studies also revealed that such a ferromagnetic contribution is preserved at temperatures well below the mean-field superconducting critical temperature of the samples (Hasanain et al. 2010; Arabi et al. 2013; Gasmi et al. 2013), raising the debate on the possible coexistence between ferromagnetism and superconductivity in these superconducting cuprates. However, there is a certain consensus that the occurrence of ferromagnetism in cuprate NPs is due to the presence of oxygen vacancies, mostly at the surface of the NPs, and their effect on the electron distribution between the atoms close to the surface (Coey et al. 2005, 2008).

As described above, much of the investigation on the general properties of nanosized superconducting cuprates has been conducted on superconducting YBCO, and a systematic study regarding the particle size effects on the magnetic properties of $Bi_{1.65}Pb_{0.35}Sr_2Ca_2Cu_3O_{10+\delta}$ (Bi-2223) material is still lacking. Thus, we describe here a systematic investigation of the structural, microstructural, and magnetic properties of ball milled powders of the superconducting cuprate Bi-2223. We have focused on the changes of the physical properties of tiny Bi-2223 powders caused by the progressive milling process and particle size reduction. Powders of single-phase Bi-2223, prepared by the traditional solid-state reaction method, were then ball milled for different times of up to 210 min and characterized by several techniques including X-ray powder diffraction (XRD), scanning electron microscopy (SEM), and transmission electron microscopy (TEM), and temperature and magnetic field dependence of the magnetic susceptibility $\chi(T, H)$.

Experimental procedure

Polycrystalline powders of $Bi_{1.65}Pb_{0.35}Sr_2Ca_2Cu_3O_{10+\delta}$ (Bi-2223) were prepared from starting oxides and carbonates Bi_2O_3, PbO, $SrCO_3$, $CaCO_3$, and CuO, which were mixed in an atomic ratio of Bi:Pb:Sr:Ca:Cu (1.65:0.35:2:2:3). The mixture was first calcined in air at 750 °C for 40 h. Then, the powder was reground and pressed into pellets of 10 mm in diameter and 2 mm in thickness at a pressure of 120 MPa. These pellets were heat treated at 800 °C in air for 40 h. Subsequently, the samples were reground, pressed again, and sintered in air at 845 °C for 40 h. This step was repeated three times, as described elsewhere (Muné et al. 2003). The obtained pellets were crushed using a mortar and pestle, and the resulting coarse powders were ground in air, at room temperature in a FRITSCH Planetary Ball Mill Pulverisette 5. Inside the mill, there is a grinding bowl (200 ml) of the tungsten carbide. We have used six grinding balls for the ball milling process: three of 10 mm diameter, and three of 20 mm. During the experiments, the initial coarse-grained mass of the Bi-2223 powder was $M_{in} \sim 30$ g, the total mass of the grinding balls was $M_b \sim 85$ g, and the rotation

velocity was $\omega = 200$ rpm. After every time interval or milling time t_m, e.g., 120, 135, 150, 165, 175, 180, and 210 min, close to ~ 1.5 g of the milled powder was separated for further physical characterizations. We have varied the ratio of the weight of balls to the mass of powder or the ball-to-powder ratio (BPR) as 5:1, 6:1, 7:1, 9:1, 14:1, 19:1, and 30:1. We will refer to these samples as M120, M135, M150, M165, M175, M180, and M210, respectively, as listed in Table 1. The pristine powder of the Bi-2223 crystal phase is termed M0.

The crystal phase evaluation of the powder samples was carried out using XRD patterns obtained in a Bruker-AXS D8 Advance diffractometer. These measurements were performed at room temperature using Cu Kα radiation in the $3^\circ \leq 2\theta \leq 80^\circ$ range with a 0.05° (2θ) step size and 5 s counting time.

The morphology of the grains was observed by using a JEOL JSM-5800 SEM operating at 25 kV. In addition to this technique, TEM was also used to gain further information regarding the morphology of the powders. The TEM images were obtained on a Philips CM 200 microscope operating at an accelerating voltage of 200 kV. From this type of micrography, we were also able to estimate the average size of the grains in our samples.

All magnetization measurements were performed in a commercial Quantum Design SQUID magnetometer in powder samples. The magnetization as a function of temperature $M(T)$ was performed under both zero-field-cooled (ZFC) and field-cooled (FC) conditions. The ZFC cycle was performed after cooling down the sample to 5 K without the application of any magnetic field. After this step, a magnetic field of $H_a = 50$ Oe was applied, and the data were collected during warming from 5 to 300 K. Subsequently, the FC measurements were performed by cooling the sample slowly from 300 K down to 5 K in the same applied magnetic field H_a. Also, the magnetization as a function of the applied magnetic field, $M(H)$, was measured in the range of $-70 \leq H \leq 70$ kOe, at selected temperatures. The magnetic susceptibility of the samples $\chi(T)$ was obtained from $M(T)/H$.

Table 1 Relevant parameters of the Bi-2223 samples studied in this work

Sample	t_m(min)	BPR	T_{min} (K)	M^{rem} (10^{-4} emu/g)
M120	120	5:1	20	2.4
M135	135	6:1	25	2.9
M150	150	7:1	30	3.5
M165	165	9:1	35	3.6
M175	175	14:1	40	4.5
M180	180	19:1	45	5.5
M210	210	30:1	92	6.6

t_m is the milling time, BPR is the ball-to-powder ratio, T_{min} is the temperature at which the $\chi(T)$ dependence attains a minimum, and M^{rem} is the remnant magnetization

Results and discussion

We start our discussion by displaying in Fig. 1 the ball-to-powder ratio (BPR) for different values of the milling time, t_m, typically ranging from 0 to 210 min. The results indicate that the values of BPR remain essentially unaltered between 0 and 120 min, indicating that little energy has been transferred to the grains during the milling time. On the other hand, after $t_m \sim 120$ min, the ball-to-powder ratio starts to increase faster with the milling time t_m, reaching its highest value of ~ 19 for the sample M210. The faster increase in the BPR versus t_m behavior, for $t_m \geq 120$ min, further indicates that the milling energy is currently being transferred to the Bi-2223 grains.

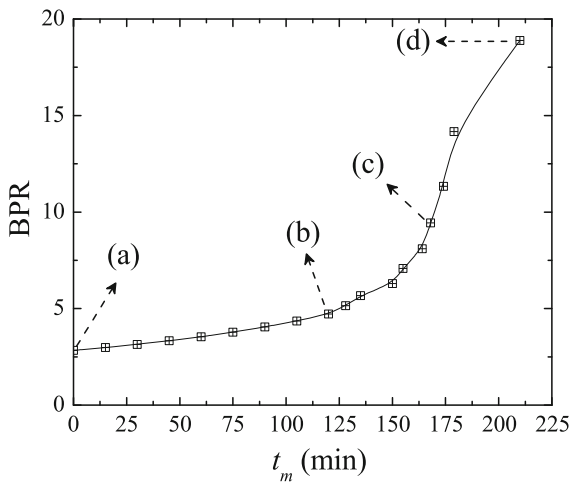

Fig. 1 Milling time, t_m, dependence of the ball-to-powder (BPR) ratio of all milled samples in this study. Selected samples *a* BM0, *b* M120, *c* M175, and *d* M210 are indicated by *arrows* (see Table 1). *Line* between points is a guide for the eyes

Under this circumstance, appreciable changes in the morphology and size of the Bi-2223 grains are expected. Taking into account these experimental results, our study is mainly focused on the physical properties of samples ball milled for milling times $t_m \geq 120$ min.

Figure 2 shows the XRD patterns taken on the starting powder and ball milled samples M0, M120, M165, M175, and M210. We first mention here that the starting powder M0 exhibits all the indexed reflections related to the high-T_c Bi-2223 phase (Muné et al. 2003). We also mention that the observed Bragg peaks are sharp, further indicating a high degree of crystallinity of the material. The unit-cell parameters were calculated regarding an orthorhombic unit cell, and the obtained values $a = 5.410$ Å, $b = 5.413$ Å, and $c = 37.152$ Å are in line with those reported elsewhere for the same compound (Muné et al. 2003). As the milling time increases, a clear broadening of the width of the Bragg peaks is observed as well as an increase of the background in the patterns, indicating a decrease in the average grain size of the powders and an increase in the degree of disorder of the milled material. Such a behavior is closely related to the increase of BPR (see Table 1).

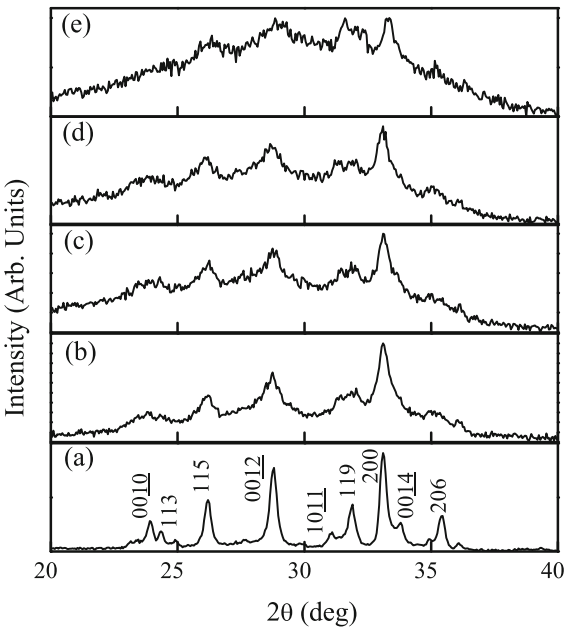

Fig. 2 X-ray diffraction patterns of samples M0 (*a*), M120 (*b*), M165 (*c*), M175 (*d*), and M210 (*e*). The Bragg reflections belonging to the Bi-2223 phase are marked by Miller indexes in (*a*)

As discussed previously, we have found that just over $t_m = 120$ min, the BPR starts to increase monotonically with milling time (see Fig. 1). In this range of milling time, the BPR will have a well-marked effect on the grain size of the samples, mostly related to an increase in the milling energy transferred to the grains. Also, it is remarkable that most of the Bragg peaks, identified in the starting powder, remain visible in the X-ray patterns of ball milled samples, even in the highly amorphized M210 sample (see Fig. 2e). These results indicate that an appreciable amount of the Bi-2223 crystal phase seems to be not altered significantly by the prolonged milling time and that the tiny grains still comprised large and coherent regions. Regardless of the occurrence of Bragg peaks belonging of the Bi-2223 phase in all samples, the XRD data indicate that a systematic decrease in the mean size of the grains with increasing milling time may be accompanied by a continuous increase of a disordered shell at their surfaces. This is particularly expected due to the high energy employed during the milling process. In addition to this, it is also probable that our samples have a low volume fraction of extra phases, as the low-T_c Bi-2212 phase for instance. The peaks of such a phase would be hardly detected due to the low intensities of their reflections, very high background of the patterns, and therefore the continuous broadening of the Bragg peaks with increasing milling time.

The morphology of the powder samples was found to be greatly altered with increasing milling time. This may be visualized in the successive SEM images of the starting powder M0 and samples M120 and M165 displayed in Fig. 3. A careful inspection of the SEM images indicates that all samples have a broad distribution of particle size and different morphologies along the series, i.e., with the progressive increase of milling time. The starting powder (see Fig. 3a) comprises platelet-like grains with dimensions of ~ 4 μm length and ~ 0.5 μm thickness. This platelet-like morphology is typical of Bi-2223 superconducting samples and results from the high anisotropic crystal structure repeatedly found in superconducting cuprates (Govea-Alcaide et al. 2007). Increasing t_m to 120 min results in appreciable changes in the morphology of the grains, as shown in the SEM images of the sample M120 displayed in Fig. 3b. The resulting M120 powder consists of a few and much smaller platelet-like grains of ≤ 1 μm and a

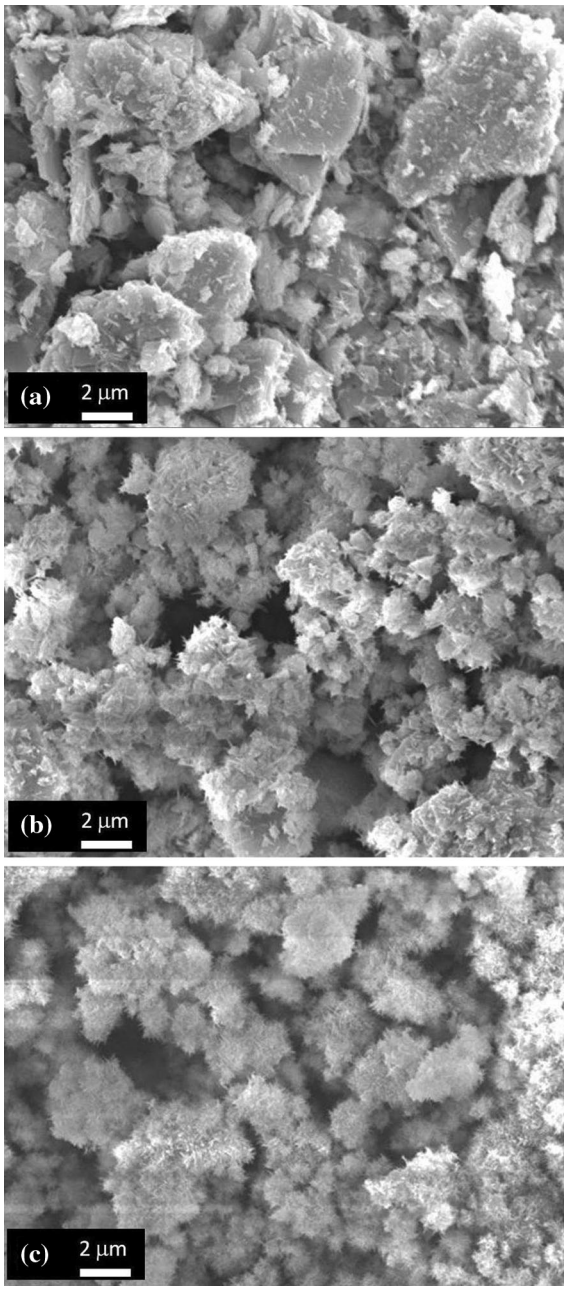

Fig. 3 SEM images for different milling times of samples: **a** the starting powder M0, **b** M120, and **c** M165

great number of very thin particles. Increasing further the milling time to 165 min results in an entirely different morphology of the Bi-2223 grains, as displayed in Fig. 3c. The SEM image of sample M165 clearly shows a very low population of the even smaller, platelet-like grains, and that the resulting powder is composed of agglomerates (or clusters) consisting of very tiny particles. It is expected that the very tiny particles have a highly disordered surface due to the high energy employed during the ball milling process. This is particularly supported by the very high background observed in the XRD powder diagrams that increases with increasing milling time (see Fig. 2). In addition to this, the formation of the tiny Bi-2223 particles is certainly related to the fracture of the large ~ 4 μm grains by different mechanisms. In this particular case, fracture by a combination of abrasion, attrition, and/or fragmentation may be responsible for such a resulting morphology (Verkoeijen et al. 2002; Gaffet et al. 1995). However, taking into account the morphology of the Bi-2223 grains and the shape of the fine resultant particles, the first two mechanisms must prevail.

Figure 4 displays a selected TEM image of the sample M165. As observed in this image, the tiny particles of this sample have the form of nanorods. We have found that the nanorods have an average diameter of $d_g \sim$ 20 nm and a length L_g in the range of 200 $\leq l \leq$ 800 nm. The occurrence of nanorod-like grains seems to be a common feature of ball milled superconducting cuprates, as reported elsewhere (Lu et al. 2007). From the images displayed in Figs. 2 and 4, it is reasonable to infer that both the number and the size of the Bi-2223 grains have a definite change with increasing milling time.

Changes in the morphology of the ball milled samples certainly have their counterparts in the magnetic properties of the samples. As far as this point is concerned, Fig. 5a displays the temperature dependence of the magnetic susceptibility $\chi(T)$ of the

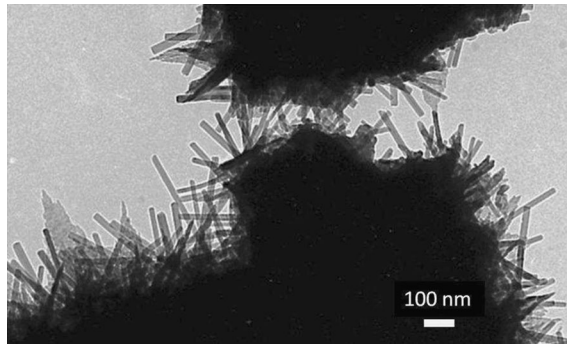

Fig. 4 TEM image of powders milled for up to t_m = 165 min, also referred to as sample M165. The image shows an expanded view of the agglomerates or clusters of the tiny Bi-2223 grains

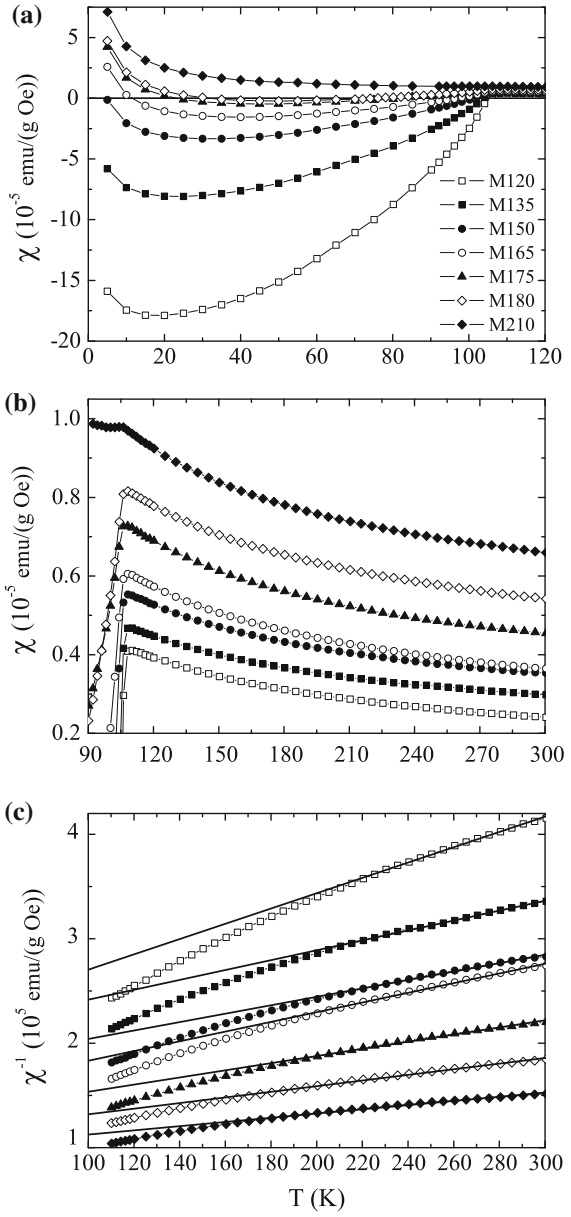

Fig. 5 Temperature dependence of the magnetic susceptibility for all samples studied in this work. **a** $\chi(T)$ curves in the superconducting region and **b** in the normal-state region. **c** The linear portion of the Curie plot, χ^{-1} versus T

ball milled samples in the superconducting region, i.e., below $\sim$110 K. Diamagnetic contributions to $\chi(T)$, indicating the occurrence of superconductivity, are observed at temperatures below $T_c \sim$ 108 K in all samples studied. We first mention that this value of $T_c \sim$ 108 K is in excellent agreement with the superconducting critical temperature reported for single-phase Bi-2223 samples with large grains (Muné et al. 2003), further indicating the presence of the Bi-2223 phase in all milled samples. We have also found that the diamagnetic signal of the ball milled samples decreases with increasing t_m. Such a successive decrease in the diamagnetic contribution to $\chi(T)$ can be understood within the framework of the London theory. For a superconducting cylinder of infinite length, with diameter d_g less than the London penetration depth λ, the magnetic susceptibility $\chi(T)$ in the superconducting region is given by $\chi(T) = -A(d_g/\lambda(T))^2$ (Shoenberg 1952), where A is a constant that takes into account the demagnetization factor of the grains and the random orientation of the particles (Paturi et al. 2003). For superconducting cuprates, typical values of $\lambda_{ab}(0) \sim$ 100–200 nm within the ab-plane and $\lambda_c(0) \sim$ 1000–7000 nm along the c-axis, and for Bi-2223 samples, $\lambda_{ab}(0) \sim$ 120 nm, are frequently found in the literature (Panagopoulos et al. 1997; Kopelevich et al. 1994). Taking our results into consideration, $d_g \ll \lambda_{ab}(0) \ll \lambda_c(0)$, and as d_g decreases systematically with increasing milling time, a continuous decrease in the diamagnetic contribution to $\chi(T)$ with t_m would be expected, in good agreement with the data displayed Fig. 5a. In addition to the decrease of the diamagnetic contribution to $\chi(T)$ with decreasing grain size, the disordered surface of the milling grains must be considered. Due to high energy of the milling process, one would also expect an increase in the degree of disorder at the surface of the ball milled grains, which may be considered as having a shell–core morphology. In such a morphology, the grains comprise a superconducting core, composed of the Bi-2223 phase, as supported by the XRD data, and a surface or shell. Such a surface or shell is expected to be highly disordered and its width to increase with increasing milling time. Such a morphology of the milled grains is sufficient for taking into account not only the systematic decrease in the diamagnetic contribution to $\chi(T)$ with increasing milling time but also other magnetic properties of the samples, as discussed below.

We have also found that below $T_c \sim$ 108 K the magnitude of the diamagnetic contribution to $\chi(T)$, displayed in Fig. 5a, increases with decreasing temperature reaching a maximum value at $T = T_{min}$. As listed in Table 1, T_{min} moves toward higher

temperatures with increasing t_m, e.g., $T_{min} \sim 20$ K in sample M120 and assumes a very high value of ~ 92 K in sample M210. In addition to this, for temperatures $T \leq T_{min}$ the magnitude of the diamagnetic signal decreases. The obtained results also show that, at $T = 5$ K, samples which were subjected to short milling times as M120, M135, and M150 still display a robust diamagnetic signal, i.e., a large superconducting fraction at low temperatures. However, in the ball milled samples for times greater than $t_m = 165$ min, the $\chi(T)$ curves exhibit a behavior of interest: the magnetic response changes from diamagnetic to paramagnetic contribution with decreasing T. This non-monotonic behavior of $\chi(T)$ indicates that the above argument, involving only the London penetration depth and changes in the dimension of the grains for supporting a continuous decrease in the diamagnetic contribution to $\chi(T)$, seems to be insufficient for explaining all the features displayed in the $\chi(T)$ curves of Fig. 5a. In fact, the experimental results strongly suggest that the very tiny Bi-2223 powders have at least two magnetic contributions to $\chi(T)$: (i) a diamagnetic one, arising from the core of the tiny grains and related to the superconducting Bi-2223 phase, and (ii) a paramagnetic contribution arising from the shell or surface of the grains. These two contributions are believed to compete with each other in a large range of T: below ~ 110 K, the magnitude of $\chi(T)$ is mainly governed by the diamagnetic contribution of the superconducting Bi-2223 phase, a feature much more pronounced in samples subjected to short milling times. This is particularly evident from the $\chi(T)$ data (see Fig. 5a) of samples M120, M135, and M150 which comprise a relatively large volume fraction of the Bi-2223 phase, i.e., large cores, and a disordered shell with a small width. In these samples, the continuous milling time is responsible for a progressive decrease in the dimensions of the grains (or cores) and an increase of the disordered surface of the grains, or more appropriately, to the shell of the tiny grains. The width of the disordered surface of the grains increases with milling time and is expected to add a paramagnetic (PL) contribution to $\chi(T)$. This PL contribution increases with decreasing T and competes with the diamagnetic one below $T_{min} \sim 110$ K, as displayed in Fig. 5a. As the milling time increases further, the large diamagnetic contribution of the cores (Bi-2223 phase) decreases not only due to the large London penetration depth λ of the materials but also due to the increase in the volume fraction of the disordered, paramagnetic shell of the tiny grains. Assuming that the diamagnetic contribution is negligible for $T \geq T_c$ and essentially constant below T_c, the minimum of $\chi(T)$ at $T = T_{min}$ and the behavior of the diamagnetic contribution as a function of T can be fully understood when a PL contribution, arising from the disordered surface of the tiny grains, that increases with increasing million time and becomes robust at low T is considered.

We have also measured the magnetic susceptibility $\chi(T)$ at 50 Oe in the normal-state region, roughly from 110 to 300 K, for all ball milled samples, and the curves are displayed in Fig. 5b. The results indicate that the qualitative behavior of all curves, except for the magnitude of the $\chi(T)$ signal, is very similar: $\chi(T)$ decreases continuously as the temperature raises, revealing the features of paramagnetic systems. However, as shown in Fig. 5c, the behavior of $1/\chi$ versus T curves does not follow the Curie–Weiss law within the entire range of T investigated. In fact, we have observed that the T window in which the $1/\chi$ versus T curves follow a linear trend increases with milling time: it is from 300 to ~ 215, 185, and 160 K in samples M120, M175, and M210, respectively, as displayed in Fig. 5c. This suggests that increasing t_m results in a large range of T in which the $1/\chi$ versus T data follow the Curie–Weiss law, a feature consistent with an increase in the volume fraction of the paramagnetic contribution to $\chi(T)$ in our samples. Such a feature is also supported by the progressive increase in the magnitude of $\chi(T)$ with increasing t_m, as shown in Fig. 5b, and is a consequence of the decrease in the average grain size and an increase in the width of the disordered shell of the tiny grains. The combined results displayed in Fig. 5a, b, and c thus indicated that at least two magnetic contributions to $\chi(T)$ data are present in the ball milled samples: (i) a diamagnetic contribution arising from the core of the grains, related to the superconducting Bi-2223 phase, and (ii) a paramagnetic contribution, arising from a disordered shell of the tiny grains.

In order to gain some insight into the origin of the paramagnetic contribution to $\chi(T)$, Fig. 5 displays hysteresis loops $M(H)$ of samples M165 and M180 measured at room temperature. The results clearly show the occurrence of magnetic hysteresis in both samples in the magnetic field range $-1 \leq H \leq 1$ kOe and that the magnetization curves are symmetric at about zero applied magnetic field, indicating the

absence of exchange bias. At higher fields, the magnetization data exhibit a paramagnetic contribution and no evidence of magnetic saturation up to 70 kOe (see insets in Fig. 6a, b). The absence of magnetization saturation in applied magnetic fields as high as 70 kOe indicates that the spins at the surface of the milled grains are contributing to the magnitude of $\chi(H)$, as observed in several families of nanostructured materials (Sundaresan and Rao 2009). We have also found that the coercivity $H_c \sim 124$ Oe at $T = 300$ K in sample M180 is greater than $H_c \sim 66$ Oe in sample M165, and therefore a systematic decrease in H_c with decreasing milling time has been observed. This is somewhat mirrored in the remnant magnetization M^{rem} for all samples listed in Table 1: M^{rem} increases with increasing milling time. This suggests a certain relationship between the strength of the ferromagnetic signal and t_m, or more appropriately the BPR.

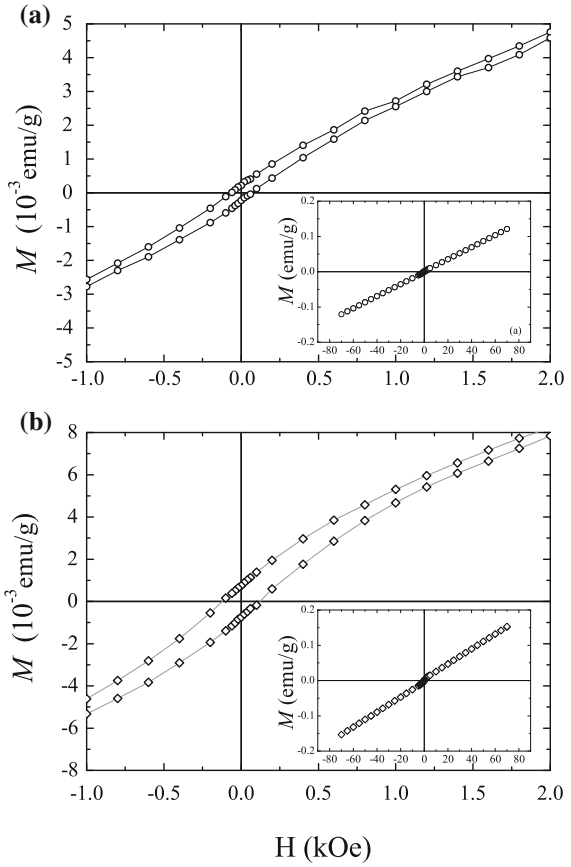

Fig. 6 M versus H curves measured in samples M165 (**a**) and M180 (**b**) at $T = 300$ K (**b**). The *insets* display the overall behavior of these curves in the range $-70 \leq H \leq 70$ kOe

At first glance, the occurrence of a magnetic hysteresis in $M(H)$ curves indicates a ferromagnetic contribution to $\chi(T)$ in the ball milled samples. However, it is difficult to attribute the ferromagnetic contribution, extracted from the $M(H)$ curves, to a genuine ferromagnetic phase in the milled samples studied here. This is because it is well known that *superconducting* samples of copper oxide do not exhibit long-range ferromagnetic order as well as no longer ferromagnetic extraphases (Sonier et al. 2010). In fact, the possibility of a ferromagnetic ordering in heavily overdoped, not superconducting, Bi-2201 single crystals has been raised due to the occurrence of a van Hove singularity detected by scanning tunneling spectroscopy experiments (Piriou et al. 2011). The results indicated ferromagnetic fluctuations in metallic Bi-2201 due to an increase in the density of states at the Fermi level and a possible ferromagnetic transition below 2 K (Sonier et al. 2010). We also mention that the CuO planes of superconducting cuprates may also develop weak ferromagnetism at the interfaces with ferromagnetic oxides due to the charge transfer of spin-polarized electrons from the ferromagnetic thin film which seems to be not the case here (De Luca et al. 2014).

One may also consider the source of the ferromagnetic-like contribution to $M(T)$ data to the formation of CuO nanograins or even CuO nanorods and nanowires during the milling process. As far as this point is concerned, the magnetic properties of CuO nanograins and CuO nanowires, synthesized by the electrical resistive heating method, may be considered (Souza et al. 2013). The authors have found a ferromagnetic-like contribution to $M(T)$ data, for magnetic fields $H > 5$ kOe, in these CuO structures. However, the magnitude of the magnetic signal found in $M(T)$ at magnetic fields $H > 5$ kOe was, at least, two orders of magnitude smaller than the ones observed here at 0.5 kOe or even lower. These two features, identified as arising from tiny CuO structures (Souza et al. 2013), are hardly seen in the data displayed in Figs. 5 and 6. In addition to this, the occurrence of either CuO nanograins or CuO nanowires will be easily detected by X-ray diffraction due to well-defined Bragg peaks occurring in the range $30 \leq 2\theta \leq 40°$, a feature absent in our X-ray diffraction data displayed in Fig. 2.

Thus, it is most likely that such a ferromagnetic contribution has its origin in the disordered and oxygen-deficient surface of the milled grains. It is

well known that oxygen nonstoichiometry at the surface of grains in Bi-2223 is not only responsible for changes in the magnetic properties of the samples but also for a strong decrease of its superconducting critical temperature (Govea-Alcaide et al. 2015). Therefore, disordered surfaces and oxygen nonstoichiometry, as the result of the ball milling process, may display a charge transfer ferromagnetism in defect-rich regions of oxide surfaces (Coey et al. 2008; Goya and Rechenberg 1999). Such a ferromagnetic contribution to $\chi(T, H)$ has been found in nanoparticles and thin films of diluted magnetic oxides and other systems with disordered and nonstoichiometric surfaces, similar to those seen in our milled materials (Coey et al. 2008; Goya and Rechenberg 1999).

In summary and by taking into account all the experimental results described above, it is reasonable to infer that the magnetic behavior of the ball milled Bi-2223 samples may be understood by assuming three different magnetic contributions to $\chi(T)$ in a large range of T: (i) a diamagnetic contribution, associated with a superconducting Bi-2223 phase; (ii) a paramagnetic contribution, arising from the disordered shell of the milled grains; and (iii) a ferromagnetic contribution related to the disordered and oxygen-deficient surface of the grains. These different contributions to the $\chi(T)$ manifest themselves within different ranges of temperatures and applied magnetic fields. At room temperature, for instance, the ferromagnetic contribution to $\chi(T)$ is robust in samples milled for prolonged times and in the low-magnetic field region ($H \leq$ 2 kOe). Below $\sim$110 K, the diamagnetic contribution of the samples milled for short times dominates the magnetic behavior of $\chi(T)$. All these magnetic behaviors are related with the milling process, i.e., the superconducting, or diamagnetic contribution to $\chi(T)$ decreases with increasing milling time or more appropriately to the BPR. The increase of the milling energy has a definite effect on the grain size and the surface of the grains (Goya and Rechenberg 1999). As the grain size decreases, the diamagnetic contribution to $\chi(T)$ becomes weaker, and under this circumstance the paramagnetic contribution to $\chi(T)$, including the ferromagnetic contribution from the oxygen-deficient surface of the grains, emerges. The origin of the later contribution seems to be related to surface defects created during the ball milling process (Sundaresan and Rao 2009; Goya and Rechenberg 1999). In the milling process, the surface of the grains is submitted to extreme conditions, allowing the formation of oxygen vacancies (Coey et al. 2008; Goya and Rechenberg 1999). It is expected that the ball milling process leads to the occurrence of Bi-2223 nanorods with a shell–core structure comprising (i) a core of stoichiometric Bi-2223 phase and (ii) a disordered shell in which its surface is rich in oxygen vacancies. The results indicate that the number of defects, as oxygen vacancies for instance, at the surface of the grains and likely the width of the shell increase with increasing BPR.

Conclusions

We have prepared $Bi_{1.65}Pb_{0.35}Sr_2Ca_2Cu_3O_{10+\delta}$ (Bi-2223) nanopowders using the high-energy ball milling technique. The ball milling process does not affect appreciably the phase content of the samples but has a well-marked influence in the size and morphology of the Bi-2223. We have found that the milling process results in grains with nanorod morphology when milled for times higher than 120 min and with a ball-to-powder ratio greater than 5:1. Besides this, the grains have a shell–core morphology in which the core comprises the Bi-2223 phase and a disordered, oxygen-deficient shell. The width of the disordered shell is believed to increase with increasing milling time as well as its surface oxygen deficiency. This kind of morphology of the grains has a significant effect on their magnetic properties. At the first stages of the milling process, the large grains are reduced to tiny particles and a well-defined decrease in the diamagnetic contribution, related to the volume fraction of the superconducting Bi-2223 phase, to $\chi(T)$ is observed. Increasing the milling time or the energy transferred to the grains results in the creation of a disordered shell and defects, as oxygen vacancies, at its surface. Under these conditions, the diamagnetic contribution of the milled grains to $\chi(T)$ decreases continuously giving rise to a paramagnetic contribution which competes with the diamagnetic one at low temperatures. We have also found that at high temperatures or close to room temperature a ferromagnetic contribution to $\chi(T)$ is observed and associated with the oxygen vacancies located at the surface of the grains.

Acknowledgments The authors acknowledge financial support from the Brazil's agencies FAPESP (Grant No. 2013/07296-2 and 2014/19245-6) and CNPq (Grant No. 2014/444712-3). This article is dedicated to the memory of our colleague and friend, Ph.D. Enrique Pérez-Delfín (1974–2012).

References

Arabi H, Jamshidi S, Komeili N, Amirabadizadeh A (2013) Coexistence of superconductivity and ferromagnetic phases in $YBa_2Cu_3O_{7-\delta}$ nanoparticles. J Supercond Nov Magn 26:2069–2071

Black CT, Ralph DC, Tinkham M (1996) Spectroscopy of the superconducting gap in individual nanometer-scale aluminum particles. Phys Rev Lett 76:688–691

Bose S, Raychaudhuri P, Banerjee R, Vasa P, Ayyub P (2005) Mechanism of the size dependence of the superconducting transition of nanostructured Nb. Phys Rev Lett 95: 147003–147007

Coey JMD, Venkatesan M, Fitzgerals CB (2005) Donor impurity band exchange in dilute ferromagnetic oxides. Nat Mater 4:173–179

Coey JMD, Wongsaprom K, Alaria J, Venkatesan M (2008) Charge-transfer ferromagnetism in oxide nanoparticles. J Phys D 41:134012–134018

De Luca GM, Ghiringhelli G, Perroni CA, Cataudella V, Chiarella F, Cantoni C, Lupini AR, Brookes NB, Huijben M, Koster G, Rijnders G, Salluzzo M (2014) Ubiquitous long-range antiferromagnetic coupling across the interface between superconducting and ferromagnetic oxides. Nat Commun 5:5626-1–5626-7

Di Lorenzo A, Fazio R, Hekking FWJ, Falci G, Mastellone A, Giaquinta G (2000) Re-entrant spin susceptibility of a superconducting grain. Phys Rev Lett 84:550–553

Gaffet S, Abdellaoui M, Malhouroux-Gaffet N (1995) Formation of nanostructural materials induced by mechanical processings. Mater Trans JIM 36:198–209

Gasmi M, Khene S, Fillion G (2013) Coexistence of superconductivity and ferromagnetism in nanosized YBCO powders. J Phys Chem Solids 74:1414–1418

Govea-Alcaide E, García-Fornaris I, Muné P, Jardim RF (2007) Improvement of the intergranular pinning energy in uniaxially compacting $(Bi-Pb)_2Sr_2Ca_2Cu_3O_{10+\delta}$ ceramic samples. Eur Phys J B 58:373–378

Govea-Alcaide E, Machado IF, Jardim RF (2015) 10 to 25-fold increase in the transport superconducting critical current density of spark-plasma sintered Bi-2223 superconductors. J Appl Phys 117:043903-1–043903-5

Goya GF, Rechenberg HR (1999) Magnetic properties of $ZnFe_2O_4$ synthesized by ball milling. J Magn Magn Mater 203:141–142

Hasanain SK, Akhtar N, Mumtaz A (2010) Particle size dependence of the superconductivity and ferromagnetism in YBCO nanoparticles. J Nanopart Res 13:1953–1960

Kopelevich Y, Moehlecke S, Torres JHS (1994) Flux-line-lattice melting in $Bi_2Sr_2Ca_2Cu_3O_{10}$. Phys Rev B 49:1495–1498

Lu XL, Zhang GQ, Qu JF, Wang W, Zhang YQ, Li XG (2007) From nanorods to nanowires: a controllable synthesis of one-dimensional superconducting cuprates. Phys C 460: 1438–1440

Muné P, Govea-Alcaide E, Jardim RF (2003) Influence of the compacting pressure on the dependence of the critical current with magnetic field in polycrystalline $(Bi-Pb)_2Sr_2Ca_2Cu_3O_x$ superconductors. Phys C 384:491–500

Panagopoulos C, Cooper JR, Xiang T, Peacock GB, Gameson I, Edwards PP (1997) Probing the order parameter and the *c*-axis coupling of high-T_c cuprates by penetration depth measurements. Phys Rev Lett 79:2320–2323

Paturi P, Raittila J, Huhtinen H, Huhtala V-P, Laiho R (2003) Size-dependent properties of $YBa_2Cu_3O_{6+x}$ nanopowder. J Phys 15:2103–2114

Piriou A, Jenkins N, Berthod C, Maggio-Aprile I, Fischer O (2011) First direct observation of the Van Hove singularity in the tunnelling spectra of cuprates. Nat Commun 2:221

Ralph DC, Black CT, Tinkham M (1995) Spectroscopic measurements of discrete electronic states in single metal particles. Phys Rev Lett 74:3241–3244

Reich S, Leitus G, Popovitz-Biro R, Schechter M (2003) Magnetization of small lead particles. Phys Rev Lett 91: 147001–147005

Shipra Gomathi A, Sundaresan A, Rao CNR (2007) Room temperature ferromagnetism in nanoparticles of superconducting materials. Solid State Commun 142:685–688

Shoenberg D (1952) Superconductivity. Cambridge University Press, Cambridge, p 134

Sonier JE, Kaiser CV, Pacradouni V, Sabok-Sayr SA, Cochrane C, MacLaughlin DE, Komiya S, Hussey NE (2010) Direct search for a ferromagnetic phase in a heavily overdoped nonsuperconducting copper oxide. Proc Natl Acad Sci USA 107:1713117134

Souza JA, Criado D, Zuniga A, Miranda VN, Ramirez FEN, Masunaga SH, Jardim RF (2013) Enhanced ferromagnetism in CuO nanowires on the top of CuO nanograins. J Appl Phys 114:173907-1–173907-7

Sundaresan A, Rao CNR (2009) Implications and consequences of ferromagnetism universally exhibited by inorganic nanoparticles. Solid State Commun 149:1197–1200

Sundaresan A, Rao CNR (2009) Ferromagnetism as a universal feature of inorganic nanoparticles. Nano Today 4:96–106

Verkoeijen D, Meesters G, Vercoulen P, Scarlett B (2002) Determining granule strength as a function of moisture content. Powder Technol 124:195–200

Von Delft J (2001) Superconductivity in ultrasmall metallic grains. Ann Phys 10:1–60